

ThermoHands: A Benchmark for 3D Hand Pose Estimation from Egocentric Thermal Image

Fangqiang Ding^{1,†}, Yunzhou Zhu^{1,†}, Xiangyu Wen¹, and Chris Xiaoxuan Lu^{2,*}

¹ University of Edinburgh, Edinburgh, UK

² University College London, London, UK

† Equal contribution. * Corresponding author

Abstract. In this work, we present ThermoHands, a new benchmark for thermal image-based egocentric 3D hand pose estimation, aimed at overcoming challenges like varying lighting and obstructions (e.g., handwear). The benchmark includes a diverse dataset from 28 subjects performing hand-object and hand-virtual interactions, accurately annotated with 3D hand poses through an automated process. We introduce a bespoke baseline method, TheFormer, utilizing dual transformer modules for effective egocentric 3D hand pose estimation in thermal imagery. Our experimental results highlight TheFormer’s leading performance and affirm thermal imaging’s effectiveness in enabling robust 3D hand pose estimation in adverse conditions.

1 Introduction

Egocentric 3D hand pose estimation is critically important for interpreting hand gestures across various applications, ranging from extended reality (XR) [48, 57, 69, 93], to human-robot interaction [21, 22, 71], and to imitation learning [1, 13, 66]. Its importance has been magnified with the advent of advanced XR headsets such as the Meta Quest series [58] and Apple Vision Pro [2], where it serves as a cornerstone for spatial interaction and immersive digital experiences.

While current research of hand pose estimation primarily focuses on RGB image-based methods [15, 20, 47, 49, 92], these approaches are particularly vulnerable to issues related to lighting variation and occlusions caused by handwear, e.g., gloves or large jewellery [3, 86]. These challenges underscore the imperative for robust egocentric 3D hand pose estimation capable of performing reliably in a variety of common yet complex daily scenarios. The prevailing approach to facilitate robust hand pose estimation in low-light conditions utilizes *near infrared* (NIR) cameras paired with active NIR emitters. This technology, invisible to the human eye, leverages active NIR emitter-receiver configurations for depth estimation through time-of-flight (ToF) or structured lighting. Nevertheless, active NIR systems are more power-intensive compared to passive sensing technologies [32, 33] and are prone to interference from external NIR sources, such as sunlight [84] and other NIR-equipped devices [75]. Consequently, these vulnerabilities restrict the effectiveness of hand pose estimation under bright

daylight conditions and in situations where multiple augmented reality (AR) or virtual reality (VR) systems are used for collaborative works.

In contrast to NIR-based methods, thermal imaging cameras offer a passive sensing solution for hand pose estimation by capturing long-wave infrared (LWIR) radiation emitted from objects, thereby eliminating reliance on the visible light spectrum [54]. This unique attribute of thermal imaging introduces several benefits for 3D hand pose estimation. Primarily, it accentuates the hand’s structure via temperature differentials, negating the effects of lighting variability. Moreover, thermal cameras are capable of detecting hands even under handwear such as gloves by identifying heat transmission patterns. This ability ensures a stable and consistent representation of hands, independent of any coverings, thereby broadening the scope and reliability of hand pose estimation across various scenarios.

Building on the above insights, this study probes the following research question: *Can egocentric thermal imagery be effectively used for 3D hand pose estimation under various conditions (such as different lighting and handwear), and how does it compare to techniques using RGB, NIR, and depth³ spectral imagery?* To answer this, we introduce **ThermoHands**, the first benchmark specifically tailored for egocentric 3D hand pose estimation utilizing thermal imaging. This benchmark is supported by a novel multi-spectral and multi-view dataset designed for egocentric 3D hand pose estimation and is unique in comprising thermal, NIR, depth, and RGB images (*cf.* Tab. 1). Our dataset emulates real-world application contexts by incorporating both hand-object and hand-virtual interaction activities, with participation from 28 subjects to ensure a broad representation of actions (*cf.* Fig. 1). To offer a thorough comparison across spectral types, we gather data under five distinct scenarios, each characterized by varying environments, handwear, and lighting conditions (*cf.* Tab. 2). Considering the challenges associated with manually annotating large-scale 3D hand poses, we developed an automated annotation pipeline. This pipeline leverages multi-view RGB and depth imagery to accurately and efficiently generate 3D hand pose ground truths through optimization based on the MANO model [68] (*cf.* Fig. 3).

Together with the multi-spectral dataset, we introduce a new baseline method named *TheFormer*, specifically designed for thermal image-based egocentric 3D hand pose estimation (*cf.* Fig. 4). This approach is notable for its two parallel transformer modules, *i.e.*, mask-guided spatial transformer and temporal transformer, which encode spatio-temporal relationship for 3D hand joints without losing the computation efficiency. Our validation process begins with verifying the annotation quality, which averages an accuracy of 1cm (*cf.* Tab. 3). We then benchmark *TheFormer* against leading methods (*cf.* Tab. 4) and compare the performance of various spectral images (*cf.* Tab. 5 and Fig. 6). The findings underscore thermal imagery’s advantages in difficult lighting conditions and when hands are gloved, showing superior performance and better adaptability to challenging settings than other spectral techniques. Our main contributions are summarized as follows:

³ For readability, we treat depth and NIR as two ‘spectra’, despite their usual overlap.

- We introduce the first-of-its-kind benchmark, dubbed **ThermoHands**, to investigate the potential of thermal imaging for egocentric 3D hand pose estimation.
- We collected a diverse dataset comprising approximately 96,000 synchronized multi-spectral, multi-view images capturing hand-object and hand-virtual interactions from 28 participants across various environments. This dataset is enriched with 3D hand pose ground truths through an innovative automatic annotation process.
- We introduce a new baseline method, termed *TheFormer*, and implement two state-of-the-art image-based methods on our dataset for benchmarking.
- Based on the ThermoHands benchmark, we conduct comprehensive experiments and analysis on TheFormer and state-of-the-art methods.
- We will release our dataset, code and models and maintain the benchmark to serve as a new challenge in 3D hand pose estimation.

2 Related Works

2.1 3D Hand Pose Datasets

Datasets with 3D hand pose annotations are imperative for training and evaluating *ad-hoc* models. Existing datasets, according to their approaches of annotation acquisition, can be summarized as four types in general, *i.e.*, marker-based [18, 23, 85, 97], synthetic [29, 61–63, 103], manual [63, 83] or hybrid [11, 52, 60, 64, 104], and automatic [7, 27, 45, 76] annotated datasets. Marker-based approaches, using magnetic sensor [23, 97] or Mocap markers [18, 85], can alter and induce bias to the hand appearance. Synthetic data [29, 61–63, 103] suffers from the *sim2real* gap in terms of hand motion and texture features. Introducing human annotators to fully [63, 83] or partly [11, 52, 60, 64, 104] annotate 2D/3D keypoints circumvents the issues above, but it either limits the scale of datasets or manifests costly and laborious in practice. Most similar to ours, some datasets adopt fully automatic pipelines to obtain 3D hand pose annotations [7, 27, 45], which leverage pre-trained models (*e.g.* OpenPose [10]) to infer the prior hand information and rely on optimization to fit the MANO hand model [68].

Despite the existing progress, previous datasets only provide depth [62, 97], RGB images [60, 61, 64, 104] or both of them [7, 11, 23, 27, 29, 45, 52, 63, 83, 85, 103] as the input spectra, unable to support the study of NIR or thermal image-based 3D hand pose estimation. ThermoHands fills the gap by providing a moderate amount of multi-spectral image data, from infrared to visual light, paired with depth images. Moreover, we capture bimanual actions from both egocentric and exocentric viewpoints and design hand-object as well as hand-virtual interaction actions to facilitate a wide range of applications. Tab. 1 shows a comprehensive comparison between the existing datasets (in chronological order) and ours.

2.2 Image-based 3D Hand Pose Estimation

As a key computer vision task, 3D hand pose estimation from images is highly demanded by applications like XR [48, 57, 69, 93], human-robot interaction [21,

Table 1: Comparison of ThermoHands with existing image-based hand datasets with 3D pose annotations. (*) The number of synchronized frames of images. (**) No markers or sensors are attached to hands during data creation or capture.

Dataset	(*)frames	(**)markless	depth	thermal	real	ego	exo	two-hand	hand-obj	int	hand-virt	int
BigHands2.2M [97]	2.2M	✗	✓	✗	✓	✓	✓	✗	✗		✓	
SynthHands [63]	220K	✓	✓	✗	✗	✓	✓	✗	✓			✗
EgoDexter [63]	3K	✓	✓	✗	✓	✓	✗	✗	✓			✗
FPHA [23]	105K	✗	✓	✗	✓	✓	✗	✗	✓			✗
ObMan [29]	150K	✓	✗	✗	✗	✗	✓	✗	✓			✗
FreiHAND [104]	37K	✓	✗	✗	✓	✗	✓	✗	✓			✓
HO-3D [27]	78K	✓	✓	✗	✓	✗	✓	✗	✓			✗
ContactPose [7]	2.9M	✓	✓	✗	✓	✗	✓	✓	✓			✗
InterHand2.6M [60]	2.6M	✓	✗	✗	✓	✗	✓	✓	✗			✓
H2O [45]	571K	✓	✓	✗	✓	✓	✓	✓	✓			✗
DexYCB [11]	508K	✓	✓	✗	✓	✗	✓	✗	✓			✗
HOI4D [52]	2.4M	✓	✓	✗	✓	✓	✗	✗	✓			✗
AssemblyHands [64]	3.0M	✓	✗	✗	✓	✓	✓	✓	✓			✗
ARCTIC [18]	2.1M	✗	✗	✗	✓	✓	✓	✓	✓			✗
ThermoHands (ours)	96K	✓	✓	✓	✓	✓	✓	✓	✓			✓

[22, 71] and imitation learning [1, 13, 66]. Therefore, this field has been extensively explored in previous arts that uses single RGB [4, 6, 14, 29, 35, 39, 47, 49, 51, 60, 80, 82, 91, 96, 98, 99] or depth [24, 59, 94, 100, 101] image as input. These methods can be roughly categorized into two fashions, *i.e.*, model-based and model-free methods. Model-based methods [4, 6, 29, 47, 51, 80, 91, 98, 99] utilize the prior knowledge of the MANO hand model [68] by estimating its shape and pose parameters, while model-free methods [14, 24, 35, 39, 49, 59, 60, 82, 94, 96, 100, 101] learn the direct regression of 3D hand joints or vertices coordinates. Recently there has been growing interest in leveraging the temporal supervision [28, 43, 51, 65, 95] or leveraging sequential images as input [9, 15, 16, 20, 37, 92] for 3D hand pose estimation. In this study, we evaluate existing methods and our baseline method in both single image-based and video-based problem settings, respectively. Apart from the previous approaches, we investigate the potential of thermal imagery for tackling various challenges in 3D hand pose estimation.

2.3 Thermal Computer Vision

Thermal cameras achieve imaging by capturing the radiation emitted in the LWIR spectrum and deducing the temperature distribution on the surfaces [54]. Leveraging its robustness to variable illumination and unique temperature information, numerous efforts have been made to address various computer vision tasks, including super-resolution [25, 36, 67], human detection [8, 26, 34], action recognition [5, 17] and pose estimation [12, 56, 81], semantic segmentation [41, 44, 46, 89], depth estimation [40, 55, 77, 78], visual(-inertial) odometry/SLAM [38, 72, 73, 79], 3D reconstruction [50, 70, 74], *etc.* In this work, we focus on 3D hand pose estimation, which is an under-exploited task based on thermal images.

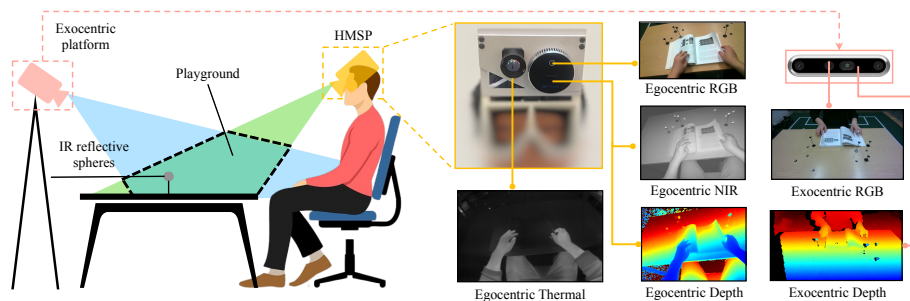


Fig. 1: Data capture setup with the HMSP and exocentric platform recording multi-view multi-spectral images of two-hand actions performed by participants.

3 The ThermoHands Benchmark

3.1 Multi-Spectral Hand Pose Dataset

Overview. At the core of our benchmark lies a multi-spectral dataset for 3D hand pose estimation (*cf.* Tab. 2), capturing hand actions performed by 28 subjects of various ethnicities and genders⁴. As shown in Fig. 1, we develop a customized head-mounted sensor platform (HMSP) and an exocentric platform to record multi-view data. During capture, our participants are asked to perform pre-defined hand-object and hand-virtual interaction actions within the playground above the table. The main part is captured in the well-illuminated office scenario. To facilitate the evaluation under different settings, four auxiliary parts are recorded i) under the darkness, ii) under the sun glare, iii) with gloves on hand, and iv) in the kitchen environment with different actions, respectively.

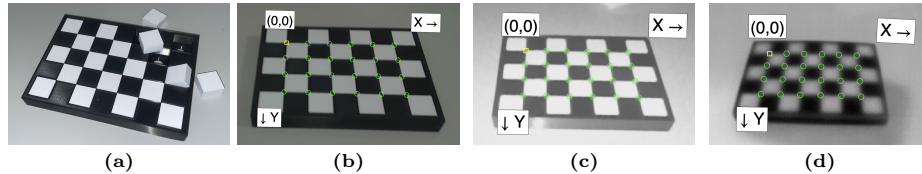
Sensor Platforms. The HMSP is mounted with an Intel RealSense L515 LiDAR depth camera [33] streaming egocentric RGB, depth and NIR images, and a FLIR Boson 640 thermal camera [87] receiving the LWIR to obtain the thermal images. To better simulate XR devices, the HMSP is modularly designed as two components: a base and a sensor board with a fixed 30-degree downward tilt. An extra exocentric platform equipped with an Intel RealSense D455 [32] is leveraged to support multi-view annotation (*cf.* Sec. 3.2) as well as provide the RGB-D image data from the third-person viewpoint. As exhibited in Fig. 1, we place the two depth sensors outside each other’s FoV to minimize interference caused by their NIR emitters [32, 33]. In the office environment, random heat sources, *e.g.*, servers and chargers, are strategically placed in the background to increase realism and introduce challenging factors into thermal images.

Synchronization. We use a single PC to simultaneously gather data streams from two sensor platforms, ensuring the synchronization of their timestamps. After collection, we synchronize six types of images, each with distinct frame rates, w.r.t. the timestamps of thermal images (8.5fps), thereby generating synchronized multi-spectral, multi-view data samples as our released data.

⁴ The study has received the ethical approval from XXX (no name for blind review), and participant consent forms were signed before the collection.

Table 2: Benchmark Dataset Statistics. The overall duration of our dataset is over 3 hours with $\sim 96\text{K}$ synchronized frame of all types of images collected.

Setting	Well-illuminated office (Main)				Other settings				Total
	train	val	test	sum	darkness	sun glare	gloves	kitchen	
#frames	47,436	12,914	24,002	84,352	3,188	2,508	3,068	2,808	95,924
#seqs	172	43	86	301	12	12	12	14	352
#subjects	16	4	8	28	1	1	1	2	-

**Fig. 2: Thermal calibration chessboard** containing a black base board and multiple removable white cubes (a). By cooling down the base board, it shows similar patterns and allows automatic corner detection in all (b) RGB, (c) NIR and (d) thermal images.

Calibration. For accuracy, we use factory-calibrated intrinsic parameters from the D455 and L515 cameras [32, 33]. To better calibrate the parameters of the thermal camera, we self-design a modular calibration chessboard as shown in Fig. 2. Before calibration, we cool down the black base board while keeping the white cubes at room temperature to create a visible chessboard pattern in all three spectra, which can be seen in Fig. 2. In this way, we can simultaneously calibrate the intrinsic parameter of the thermal camera and its extrinsic parameter w.r.t. the L515 camera. To enable the calibration between the two viewpoints, we place 11 IR reflective spheres at random locations and heights above the table. At the first frame of each sequence, we manually annotate their 2D locations from two viewpoints, retrieve their depth values and compute the transformation between two viewpoints by solving the PnP [19]. For the subsequent frames, the KISS-ICP [90] odometry method is used to track the motion of the ego-head using the point clouds converted from the egocentric depth images.

Dataset Statistics. As shown in Tab. 2, our dataset consists of approximately 96K synchronized multi-spectral multi-view frames (*cf.* Fig. 1) and 352 independent sequences in total. The main part is collected under the well-illuminated office scenario, where each participant⁵ performs 7 scenario-specific hand-object interaction actions: *cut paper*, *fold paper*, *pour water*, *read book*, *staple paper*, *write with pen*, *write with pencil*, and 5 hand-virtual interaction actions: *pinch and drag*, *pinch and hold*, *swipe*, *tap*, *touch*, with two hands. This main part is divided into the training, validation and testing splits by subjects with a ratio of 4:1:2. We also collect four auxiliary testing sets by asking one subject to perform the aforementioned 12 actions in the darkness, sun glare and gloves settings individually, and two subjects to perform 7 scenarios-specific interaction

⁵ Due to their limited time, 7 participants only perform the hand-object actions.

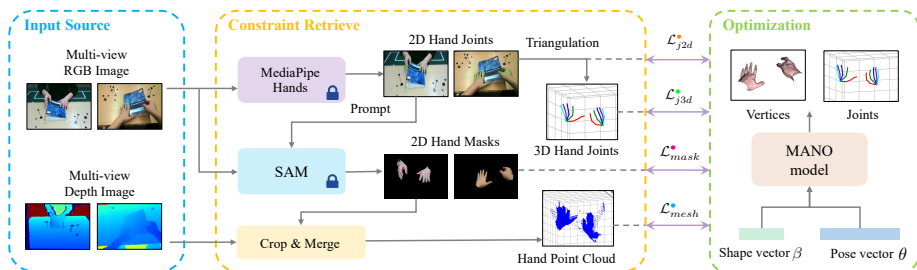


Fig. 3: Automatic annotation pipeline of 3D hand pose. We utilize the multi-view RGB and depth images as the input source and retrieve both 2D and 3D constraint information. Various error terms are formulated to optimize the MANO parameters.

actions: *cut*, *spray*, *stir*, *wash hands*, *wash mug*, *wash plate*, *wipe* in the kitchen environment. Please refer to the supplementary for more dataset details.

3.2 Hand Pose Annotation

To refrain from employing tedious human efforts for annotation, we implement a fully automatic annotation pipeline, similar to the approaches in [7, 27, 45], to obtain the 3D hand pose ground truth for our dataset.

In particular, we use the MANO statistical hand model [68] to represent 3D hand pose. The MANO model parameterizes the hand mesh vertices $\mathcal{V}(\beta, \theta)$ into two low-dimensional embeddings, *i.e.*, the shape parameters $\beta \in \mathbb{R}^{10}$ and the pose parameters $\theta \in \mathbb{R}^{51}$, consisting of 45 parameters accounting for 15 hand joint angles (3 DoF for each) plus the rest for global rotation and translation. Following the MANO PyTorch version in [30], we denote the $N_{\mathcal{J}} = 21$ hand joints mapped from the hand parameters as $\mathcal{J}(\beta, \theta)$. The MANO fitting is performed by minimizing the following optimization objective per frame for each hand:

$$\theta^* = \arg \min_{\theta} \lambda_{j2d} \mathcal{L}_{j2d}^{\bullet} + \lambda_{mask} \mathcal{L}_{mask}^{\bullet} + \lambda_{j3d} \mathcal{L}_{j3d}^{\bullet} + \lambda_{mesh} \mathcal{L}_{mesh}^{\bullet} + \lambda_{reg} \mathcal{L}_{reg}^{\bullet} \quad (1)$$

where λ_{j2d} , λ_{mask} , λ_{j3d} , λ_{mesh} , λ_{reg} are used to balance the weight of different errors. The diagram illustrating our annotation process is shown in Fig. 3.

Initialization. For each sequence, we optimize the shape parameter β^6 together with θ only at the first frame using Eq. (1) until convergence and fix its values for the subsequent frames. We initialize the pose parameter θ for each frame using the optimization result from the last frame. This helps to accelerate the convergence as well as keep the temporal consistency.

2D Joint Error $\mathcal{L}_{j2d}^{\bullet}$. Given RGB images from N_C viewpoints, we infer 2D hand joints \mathcal{J}^{2D} using MediaPipe Hands [53] and define the 2D joint error as:

$$\mathcal{L}_{j2d}^{\bullet} = \sum_{c=1}^{N_C} \alpha_c \sum_{i=1}^{N_{\mathcal{J}}} \|\mathcal{J}_{c,i}^{2D} - \pi_c(\mathcal{J}(\theta)_i)\| \quad (2)$$

⁶ For simplicity, we omit β in Eq. (1) and subsequent equations.

where $\pi_c(\cdot)$ returns the 2D projection location for 3D position in the c -th camera viewpoint, and α_c is hyperparameter used to weigh different viewpoints.

2D Mask Error $\mathcal{L}_{mask}^\bullet$. To generate the high-quality 2D hand mask, we prompt the prevalent Segment Anything Model [42] with the 2D hand joints \mathcal{J}^{2D} and the bounding box derived from it. We penalize the distance between the hand mesh vertices $\mathcal{V}(\theta)$ and the 2D binary hand mask \mathcal{M}_c as:

$$\mathcal{L}_{mask}^\bullet = \sum_{c=1}^{N_C} \alpha_c \sum_{i=1}^{N_V} \min_j \|\mathcal{M}_{c,j} - \pi_c(\mathcal{V}(\theta)_i)\| \quad (3)$$

where $\mathcal{M}_{c,j}$ is the coordinate of j -th non-zero pixel in the mask \mathcal{M}_c .

3D Joint Error $\mathcal{L}_{j3d}^\bullet$. We triangulate the 2D joints from multiple views to lift them to 3D joints \mathcal{J}^{3D} and measure their difference to $\mathcal{J}(\theta)$, which is written as:

$$\mathcal{L}_{j3d}^\bullet = \sum_{i=1}^{N_{\mathcal{J}}} \|\mathcal{J}_i^{3D} - \mathcal{J}(\theta)_i\| \quad (4)$$

3D Mesh Error $\mathcal{L}_{mesh}^\bullet$. To better supervise the hand mesh and fasten the optimization, we generate the 3D hand pose cloud \mathcal{P} by cropping the depth image using the 2D hand mask and merging all views together. The 3D mesh error term compensates for the distance between the hand mesh and point cloud:

$$\mathcal{L}_{mesh}^\bullet = \sum_{i=1}^{N_V} \min_j \|\mathcal{P}_j - \mathcal{V}(\theta)_i\| \quad (5)$$

Regularization $\mathcal{L}_{reg}^\bullet$. To alleviate irregular hand articulation, we constrain the joint angles to pre-defined lower and upper boundaries $\underline{\theta}$ and $\bar{\theta}$:

$$\mathcal{L}_{reg}^\bullet = \sum_{i=1}^{45} (\max(\underline{\theta}_i - \theta_i, 0) + \max(\theta_i - \bar{\theta}_i, 0)) \quad (6)$$

Note that we also impose regularization to the shape parameter β during initialization. Please see details of our annotation in supplementary material.

3.3 TheFormer: A Baseline Method

Our proposed baseline method, dubbed TheFormer, learns 3D hand pose estimation from egocentric thermal images based on Transformer, as exhibited in Fig. 4. The baseline network features in its two parallel transformer modules, *i.e.*, mask-guided spatial transformer and temporal transformer, to model the spatio-temporal relationship of hand joints while being computationally efficient.

Problem Definition. We consider two problem settings: single image-based and video-based egocentric 3D hand pose estimation for our benchmark. In the former setting, we aim to estimate the 3D joint positions \mathcal{J}_t for two hands given the single thermal image \mathcal{I}_t captured for the t -th frame. For the video-based

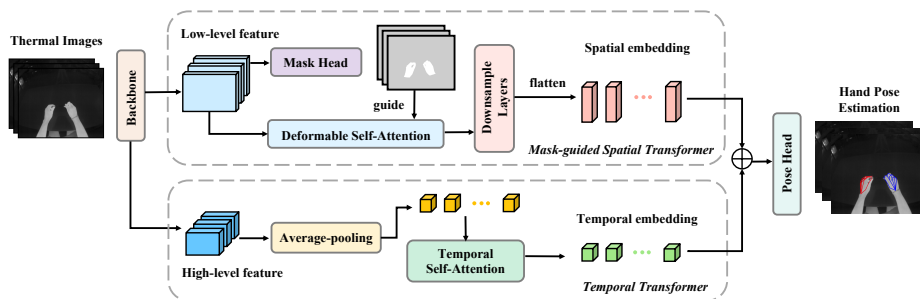


Fig. 4: Overall Framework of TheFormer. Given thermal images, we extract both low-level and high-level features for each frame, which are input to the mask-guided spatial transformer and temporal transformer. Frame-wise spatial and temporal embeddings are concatenated and fed into the pose head to regress the 3D hand pose.

one, our input is a sequence of thermal images $\mathcal{S} = \{\mathcal{I}_i\}_{i=1}^T$ and we estimate the per-frame 3D hand joint positions \mathcal{J}_i together. Compared to the single image-based counterpart, the video-based setting allows for a fully temporal interaction among sequential images, potentially offering a better performance. Nevertheless, the accumulation of sequential images leads to a higher latency for online inference, limiting its usage to applications that demand real-time hand tracking.

Network Architecture. Without losing the generality, here we illustrate our network architecture for the video-based setting. Note that our network can be flexibly adapted to the single image-based problem by setting $T = 1$. As seen in Fig. 4, given sequential thermal images, our architecture extracts the multi-level 2D feature using the backbone network per frame. We design a mask-guided spatial transformer module to enhance the spatial representation while enforcing the network to focus on the hand area. In parallel, we apply a temporal transformer module to reason the feature interaction along the temporal dimension. Both two transformers output per-frame feature embeddings that encode the spatial and temporal information, respectively. We concatenate them and use a pose head to regress the 3D coordinates of hand joints for two hands.

Backbone Features. For efficiency, we use the lightweight ResNet-18 [31] as our backbone network to extract multi-level features from thermal images. Specifically, we reserve both the low-level and high-level image features and input them to the spatial and temporal transformer modules individually. Low-level features carry fine-grained spatial details, which is crucial for accurate mask generation and spatial reasoning in our mask-guided spatial transformer. High-level features provide a broader context, helping temporal transformers to better understand the overall scene dynamics and the hand’s role within it.

Mask-guided Spatial Transformer. Human hands are highly articulated objects that can adopt a wide variety of poses, often against complex backgrounds. We propose a mask-guided spatial transformer module to accurately identify and focus on the intricacies of hand poses during spatial feature interaction. Given low-level features, we first utilize a mask head to estimate the binary hand mask in the thermal image. Then, we leverage the deformable self-attention [102] to re-

fine the hand spatial features under the guidance of the hand mask. Specifically, we only take feature elements whose spatial locations are within the hand area as queries and sample keys from only the hand area and its surrounding locations. In this way, we not only reduce the computation waste on the irrelevant region but also increase the robustness to background clutter. Lastly, we reduce the spatial dimensions of the spatial features via several downsample convolutional layers and flatten it into 1D spatial feature embedding per frame.

Temporal Transformer. Temporal information is crucial for 3D hand pose estimation when coping with occlusion and solving ambiguities. To efficiently model temporal relationships, we apply the average-pooling to the high-level features to get the global feature vector per frame. The self-attention [88] is then employed to explicitly attend to the feature vector of every frame for a comprehensive temporal interaction. Similar to the spatial transformer, the output is frame-wise feature embedding that encompasses the temporal information.

Pose Regression. We concatenate the frame-wise spatial and temporal embedding from two transformer modules and get the spatio-temporal representations for each frame. In the pose head, we use the MLP to project the representations to the output space and obtain the per-frame 3D joint output \mathcal{J}_i .

Training Loss. We leverage the binary cross-entropy loss to supervise the hand segmentation with the mask ground truth rendered from the annotated hand mesh (*cf.* Sec. 3.2). For 3D hand joint positions, we measure the $L1$ distance of its 2D projection and depth to that of the ground truth separately.

For the video-based setting, our baseline method is named as TheFormer-V, which accepts sequential images as input. The variant of our baseline to the single image-based setting is called TheFormer-S, where the temporal transformer degrades to a global transformer that only encodes the global information for a single frame. Please see the supplementary materials for more parameters, design and training details of our baseline method.

4 Experiment

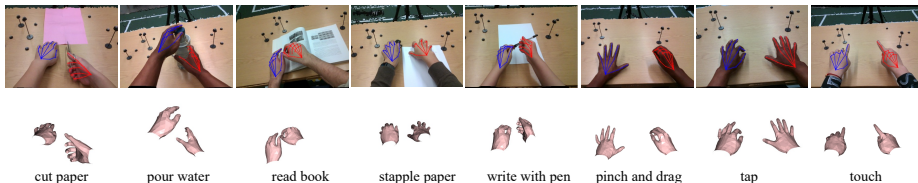
4.1 Evaluation of the Annotation Method

As the first step, we validate the accuracy of our 3D hand pose annotation and analyze the impact for optimization results. For evaluation, we manually annotate two random sequences from our main dataset: one involving hand-object interaction and the other hand-virtual interaction, with a total of over 600 frames. To that end, we first annotate the 2D joint locations from both egocentric and exocentric images and obtain the 3D positions by triangulation. We calculate the average 3D joint errors across all frames to measure the accuracy.

As shown in Tab. 3, our annotation method achieves an average joint error of nearly 1cm, comparable to the results of [27, 45, 104]. The multi-view setting shows remarkably better precision than the ego-view only optimization, demonstrating the necessity of multi-camera capture. We also observe that only combining \mathcal{L}_{mask} and \mathcal{L}_{j2d} can already provide a plausible accuracy since they fit

Table 3: Evaluation of annotation results. The average 3D joint errors across all frames are reported (in cm). \mathcal{L}_{reg} is used for all to mitigate irregular hand poses.

Errors	Ego-view optimization			Multi-view optimization		
	$\mathcal{L}_{mask} + \mathcal{L}_{j2d}$	$\mathcal{L}_{mask} + \mathcal{L}_{j2d} + \mathcal{L}_{mesh}$	\mathcal{L}_{mask}	$\mathcal{L}_{mask} + \mathcal{L}_{j2d}$	$\mathcal{L}_{mask} + \mathcal{L}_{j2d} + \mathcal{L}_{mesh}$	$\mathcal{L}_{mask} + \mathcal{L}_{j2d} + \mathcal{L}_{mesh} + \mathcal{L}_{j3d}$
mean (std)	37.29 (\pm 18.02)	7.03 (\pm 2.57)	8.13 (\pm 0.57)	1.29 (\pm 0.43)	1.28 (\pm 0.43)	1.01 (\pm 0.34)

**Fig. 5:** Examples of 3D hand pose annotations. Top row: left (blue) and right (red) hand 3D joints projected onto ego-centric RGB images. Bottom row: visualization of hand mesh annotation (defined by MANO [68]).

the projection of the 3D hand pose to two heterogeneous views. \mathcal{L}_{mesh} , though it hardly improves the joint accuracy, can result in more natural hand mesh. Adding \mathcal{L}_{j3d} further refines the joints as it induces the explicit constraint to their positions. We showcase some annotation examples in Fig. 5. As can be seen, both hand joint and mesh can be accurately annotated across different actions despite the presence of occlusion and the variance in subject ethnicities.

4.2 Benchmark Setup

Dataset Preparation. We utilize our own dataset for experiments as it uniquely contains egocentric images from multiple spectra, essentially for our benchmark experiments. We annotate the main part of our dataset (*cf.* Tab. 1) in an automatic way following Sec. 3.2, of which the training and validation sets serve as the foundation for the training of all network models.

Method and Implementation. To provide sufficient baselines for follow-up works, we selected two state-of-the-art methods in 3D hand pose estimation, *i.e.*, HTT [92] and A2J-Transformer [35], and reproduce them on our dataset for benchmark experiments. HTT [92] is a video-based method thus enabling the evaluation in both two problem settings while A2J-Transformer [35] only works under the single image-based setting. For a feasible comparison, we use the same sequence length, *i.e.*, $T = 8$, for HTT and TheFormer-V baseline. We also exclude the additional action block used by HTT [92] for hand action prediction, focusing solely on hand pose estimation. We adjusted the anchor initialization phase of the A2J-Transformer [35] to better accommodate our dataset, without altering the density of its anchors. All trained models are tested on a single NVIDIA RTX 4090 GPU for a fair comparison of their inference speed.

Evaluation Metrics. We evaluate the accuracy of 3D hand pose estimation with two metrics: *Percentage of Correct Keypoints* (PCK) and *Mean End-Point Error* (MEPE) [103], in both camera space and root-aligned (RA) space [60].

Table 4: Benchmark results of TheFormer and state-of-the-art methods on thermal-based 3D hand pose estimation. Results are reported on the main testing set. \uparrow denotes larger values are better, and vice versa. The fps displayed for sequence input indicates the number of sequences that models can process per second.

Method	Input	MEPE (mm) \downarrow	AUC \uparrow	MEPE-RA (mm) \downarrow	AUC-RA \uparrow	fps \uparrow
A2J-Transformer [35]	Single	51.68	0.474	20.76	0.603	34
HTT [92]	Single	49.09	0.489	20.69	0.599	211
TheFormer-S	Single	48.25	0.510	22.60	0.565	120
HTT [92]	Sequence	47.07	0.512	17.49	0.659	129
TheFormer-V	Sequence	46.57	0.519	19.62	0.619	67

For RA space, we align the estimated wrist with its groundtruth position before measurement. For PCK, we report the corresponding *Area Under the Curve* (AUC) over the 0-50mm/80mm error thresholds for the camera/RA space.

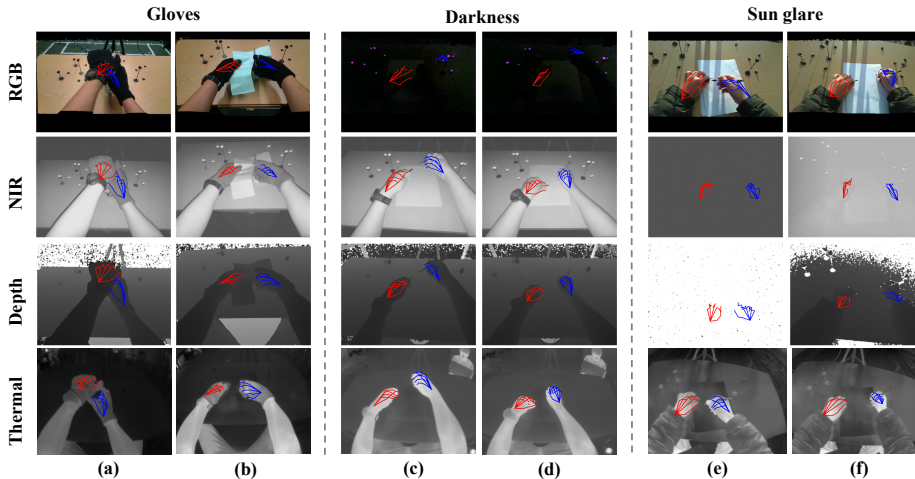
4.3 Benchmark Results

Comparison against State of the Arts. We compare the TheFormer against the state-of-the-art methods for thermal-based 3D hand pose estimation, as shown in Tab. 4. On the MEPE and AUC metrics, TheFormer-S outforms two competing methods under the single image-based setting, while TheFormer-V surpasses the counterpart HTT [92] given the same sequential images as input. Such an improvement stems from our mask-guided spatial attention design that can adaptively encode the spatial interaction among hand joints with the guidance of the hand mask (*cf.* Sec. 3.3). A performance gap can be seen between single image-based and video-based settings for both HTT [92] and TheFormer. We credit this to their usage of temporal information that helps to tackle the occlusion cases and solve ambiguities. We can also observe that TheFormer has slightly inferior results in the RA space relative to its opponents, leaving room for improvement in localizing individual hand joints once hand roots are correctly identified. This also suggests that our advancements are primarily attributed to our accurate localization of the overall hand especially the wrists. Thanks to our lightweight network design, TheFormer is highly efficient to run with fps of 120 and 67 for single and sequence input respectively, ensuring its real-time application to resource-constrained devices.

Comparison between Spectrum. To compare the efficacy of different spectra (*i.e.*, RGB, depth, NIR and thermal), we assess their performance by applying them as varying inputs to the HTT [92] and A2J-Transformer [35] method. As seen in Tab. 5, RGB spectrum yields favourable performance for both two methods as they provide rich multi-channel semantics, allowing for accurate hand pose reasoning. Specifically, A2J-Transformer [35] achieves comparable performance to HTT [92] with sequential input. This can be attributed to its usage of the larger ResNet50 [31] backbone that is pretrained with RGB images. However, this also increases the computation overhead, making A2J-Transformer [35] $6\times$ slower than HTT [92] (*cf.* Tab. 4). Depth and NIR spectra show a marginal

Table 5: Comparison between different spectra. Models are trained with their corresponding spectrum images from the training set. We test them on the main testing set.

Method	Spectrum	MEPE (mm) ↓	AUC ↑	MEPE-RA (mm) ↓	AUC-RA ↑
HTT - Sequence [92]	RGB	43.30	0.542	15.43	0.697
	Depth	41.62	0.559	17.66	0.654
	NIR	41.57	0.562	16.41	0.679
	Thermal	46.57	0.519	17.49	0.659
A2J-Transformer - Single [35]	RGB	40.21	0.577	16.77	0.675
	Depth	43.80	0.552	18.26	0.647
	NIR	46.46	0.513	18.00	0.648
	Thermal	51.68	0.474	20.76	0.603

**Fig. 6:** Examples of hand pose estimation results with various spectra under three challenging settings. For visualization, we show the projection of the estimated left (red) and right (blue) 3D hand joints on corresponding images.

decrease in performance compared to RGB in well-illuminated conditions. However, the active illumination design of NIR sensors enables them to serve as supplements to RGB in dark conditions, as illustrated in Fig. 6. The thermal spectrum, operating independently of any active light source, still achieves plausible hand pose estimation accuracy, with a small discrepancy compared to other spectra. In addition to the above evaluation on the main testing set, we show more comparison of different spectra to highlight the value of thermal images under challenging conditions for 3D hand pose estimation.

4.4 Performance under Challenging Conditions

To justify the advantages of using thermal cameras for egocentric hand pose estimation under challenging scenarios, we conduct a comparison of four spectra on three of our auxiliary testing sets, *i.e.*, gloves, darkness and sun glare (*cf.* Tab. 2). Our automatic annotation pipeline (*cf.* Sec. 3.2) becomes infeasible since

hands appear corrupted in either RGB or depth images. Therefore, we conduct a qualitative analysis of their performance and present some representative examples in Fig. 6. As can be seen, RGB-based methods fail with gloves wearing (*cf.* Fig. 6 (a-b)) and in darkness (*cf.* Fig. 6 (c-d)). Gloves change how human hands look and hide their natural colors and textures. Since RGB algorithms rely on skin’s texture and color to identify hand parts and joints, gloves, particularly those with solid colors or textures unlike skin, can interfere with this identification process. Contrary to RGB techniques, as shown in Fig. 6 (a-b), thermal imaging methods excel in identifying hands by leveraging the principles of heat conduction through gloves, effectively bypassing the limitations imposed by color and texture variations.

NIR sensors are significantly disrupted by strong sunlight, affecting both NIR imaging and depth map creation, as shown in Fig. 6 (e-f). Conversely, thermal imaging is immune to sunlight and outdoor conditions. The temperature difference between hands and their surroundings in the thermal spectrum facilitates effortless identification of the hands, leaving the thermal-based estimator unaffected. The thermal camera’s ability to consistently capture hand features in diverse lighting conditions positions it as a suitable option for future XR applications. Please see the supplementary materials for more figure examples and demo videos under challenging conditions.

5 Limitation and Future Work

Despite the advancements, we acknowledge certain limitations here guiding our future work. First, the scale of our current dataset is small when compared to some large-scale datasets [18,52,60,64] that contain millions of images (*cf.* Tab. 1). We plan to continuously enlarge this dataset by incorporating data from new scenarios and hand actions to better support future investigations in this field. Second, we only annotate 3D hand pose for our dataset, which limits its usage of evaluation to other computer vision tasks relevant to human hands. In this regard, further efforts could be directed towards a) annotating the fine-grained hand action splits inside each sequence, b) leveraging the heat residual on objects after hand grasp to annotate the contact heatmap [7] and c) generating the ground truth mesh for both rigid [45] and articulated objects [18].

6 Conclusion

This paper introduces **ThermoHands**, the first benchmark for egocentric 3D hand pose estimation using thermal images. It features a multi-spectral, multi-view dataset with automatically annotated 3D poses and a novel baseline method utilizing dual transformer modules for encoding spatio-temporal relationships. We demonstrate near 1cm annotation accuracy, show that TheFormer surpasses existing methods in thermal-based 3D hand pose estimation, and confirm thermal images’ effectiveness in challenging lighting and obstruction scenarios. We believe our endeavour could pave the way for further research in thermal-based 3D hand pose estimation and its wide application.

References

1. Antotsiou, D., Garcia-Hernando, G., Kim, T.K.: Task-oriented hand motion re-targeting for dexterous manipulation imitation. In: ECCVW (2018) **1**, **4**
2. Apple: Apple Vision Pro. <https://www.apple.com/apple-vision-pro/> (2024), accessed: 2024-02-23 **1**
3. Apple: Use gestures with Apple Vision Pro. <https://support.apple.com/en-us/117741> (2024), accessed: 2024-02-23 **1**
4. Baek, S., Kim, K.L., Kim, T.K.: Pushing the envelope for rgb-based dense 3d hand pose estimation via neural rendering. In: CVPR. pp. 1067–1076 (2019) **4**
5. Batchuluun, G., Nguyen, D.T., Pham, T.D., Park, C., Park, K.R.: Action recognition from thermal videos. *IEEE Access* **7**, 103893–103917 (2019) **4**
6. Boukhayma, A., Bem, R.d., Torr, P.H.: 3d hand shape and pose from images in the wild. In: CVPR. pp. 10843–10852 (2019) **4**
7. Brahmhatt, S., Tang, C., Twigg, C.D., Kemp, C.C., Hays, J.: ContactPose: A dataset of grasps with object contact and hand pose. In: ECCV. pp. 361–378. Springer (2020) **3**, **4**, **7**, **14**
8. Cai, K., Xia, Q., Li, P., Stankovic, J., Lu, C.X.: Robust Human Detection under Visual Degradation via Thermal and mmWave Radar Fusion. In: EWSN (2023) **4**
9. Cai, Y., Ge, L., Liu, J., Cai, J., Cham, T.J., Yuan, J., Thalmann, N.M.: Exploiting Spatial-Temporal Relationships for 3D Pose Estimation via Graph Convolutional Networks. In: ICCV (October 2019) **4**
10. Cao, Z., Hidalgo, G., Simon, T., Wei, S.E., Sheikh, Y.: OpenPose: Realtime Multi-Person 2D Pose Estimation Using Part Affinity Fields. *PAMI* **43**(1), 172–186 (2021) **3**
11. Chao, Y.W., Yang, W., Xiang, Y., Molchanov, P., Handa, A., Tremblay, J., Narang, Y.S., Van Wyk, K., Iqbal, U., Birchfield, S., et al.: DexYCB: A benchmark for capturing hand grasping of objects. In: CVPR. pp. 9044–9053 (2021) **3**, **4**
12. Chen, I.C., Wang, C.J., Wen, C.K., Tzou, S.J.: Multi-person pose estimation using thermal images. *IEEE Access* **8**, 174964–174971 (2020) **4**
13. Chen, Y., Geng, Y., Zhong, F., Ji, J., Jiang, J., Lu, Z., Dong, H., Yang, Y.: Bi-DexHands: Towards Human-Level Bimanual Dexterous Manipulation. *PAMI* (2023) **1**, **4**
14. Cheng, W., Park, J.H., Ko, J.H.: Handfoldingnet: A 3d hand pose estimation network using multiscale-feature guided folding of a 2d hand skeleton. In: ICCV. pp. 11260–11269 (2021) **4**
15. Cho, H., Kim, C., Kim, J., Lee, S., Ismayilzada, E., Baek, S.: Transformer-Based Unified Recognition of Two Hands Manipulating Objects. In: CVPR. pp. 4769–4778 (2023) **1**, **4**
16. Choi, H., Moon, G., Chang, J.Y., Lee, K.M.: Beyond static features for temporally consistent 3d human pose and shape from a video. In: CVPR. pp. 1964–1973 (2021) **4**
17. Ding, M., Ding, Y., Wei, L., Xu, Y., Cao, Y.: Individual Surveillance Around Parked Aircraft at Nighttime: Thermal Infrared Vision-Based Human Action Recognition. *IEEE Transactions on Systems, Man, and Cybernetics: Systems* **53**(2), 1084–1094 (2022) **4**
18. Fan, Z., Taheri, O., Tzionas, D., Kocabas, M., Kaufmann, M., Black, M.J., Hilliges, O.: ARCTIC: A Dataset for Dexterous Bimanual Hand-Object Manipulation. In: CVPR. pp. 12943–12954 (2023) **3**, **4**, **14**

19. Fischler, M.A., Bolles, R.C.: Random Sample Consensus: A Paradigm for Model Fitting with Applications to Image Analysis and Automated Cartography. *Communications of the ACM* **24**(6), 381–395 (1981) [6](#)
20. Fu, Q., Liu, X., Xu, R., Niebles, J.C., Kitani, K.M.: Deformer: Dynamic Fusion Transformer for Robust Hand Pose Estimation. In: *ICCV*. pp. 23600–23611 (October 2023) [1](#), [4](#)
21. Gao, Q., Chen, Y., Ju, Z., Liang, Y.: Dynamic hand gesture recognition based on 3D hand pose estimation for human–robot interaction. *IEEE Sensors Journal* **22**(18), 17421–17430 (2021) [1](#), [3](#)
22. Gao, Q., Liu, J., Ju, Z., Zhang, X.: Dual-hand detection for human–robot interaction by a parallel network based on hand detection and body pose estimation. *IEEE Transactions on Industrial Electronics* **66**(12), 9663–9672 (2019) [1](#), [3](#)
23. Garcia-Hernando, G., Yuan, S., Baek, S., Kim, T.K.: First-person hand action benchmark with rgb-d videos and 3d hand pose annotations. In: *CVPR*. pp. 409–419 (2018) [3](#), [4](#)
24. Ge, L., Liang, H., Yuan, J., Thalmann, D.: Robust 3D hand pose estimation from single depth images using multi-view CNNs. *IEEE Transactions on Image Processing* **27**(9), 4422–4436 (2018) [4](#)
25. Gupta, H., Mitra, K.: Toward unaligned guided thermal super-resolution. *TIP* **31**, 433–445 (2021) [4](#)
26. Haider, A., Shaikat, F., Mir, J.: Human detection in aerial thermal imaging using a fully convolutional regression network. *Infrared Physics & Technology* **116**, 103796 (2021) [4](#)
27. Hampali, S., Rad, M., Oberweger, M., Lepetit, V.: Honnotate: A method for 3d annotation of hand and object poses. In: *CVPR*. pp. 3196–3206 (2020) [3](#), [4](#), [7](#), [10](#)
28. Hasson, Y., Tekin, B., Bogo, F., Laptev, I., Pollefeys, M., Schmid, C.: Leveraging photometric consistency over time for sparsely supervised hand-object reconstruction. In: *CVPR*. pp. 571–580 (2020) [4](#)
29. Hasson, Y., Varol, G., Tzionas, D., Kalevatykh, I., Black, M.J., Laptev, I., Schmid, C.: Learning joint reconstruction of hands and manipulated objects. In: *CVPR*. pp. 11807–11816 (2019) [3](#), [4](#)
30. Hasson, Y., Varol, G., Tzionas, D., Kalevatykh, I., Black, M.J., Laptev, I., Schmid, C.: Learning joint reconstruction of hands and manipulated objects. In: *CVPR* (2019) [7](#)
31. He, K., Zhang, X., Ren, S., Sun, J.: Deep residual learning for image recognition. In: *CVPR*. pp. 770–778 (2016) [9](#), [12](#)
32. Intel RealSense: Depth Camera D455. <https://www.intelrealsense.com/depth-camera-d455/> (2023), accessed: 2024-02-27 [1](#), [5](#), [6](#)
33. Intel RealSense: LiDAR Camera L515. <https://www.intelrealsense.com/lidar-camera-l515/> (2023), accessed: 2024-02-27 [1](#), [5](#), [6](#)
34. Ivašić-Kos, M., Krišto, M., Pobar, M.: Human detection in thermal imaging using YOLO. In: *Proceedings of the 2019 5th International Conference on Computer and Technology Applications*. pp. 20–24 (2019) [4](#)
35. Jiang, C., Xiao, Y., Wu, C., Zhang, M., Zheng, J., Cao, Z., Zhou, J.T.: A2J-Transformer: Anchor-to-Joint Transformer Network for 3D Interacting Hand Pose Estimation from a Single RGB Image. In: *CVPR*. pp. 8846–8855 (2023) [4](#), [11](#), [12](#), [13](#)
36. Kansal, P., Nathan, S.: A multi-level supervision model: A novel approach for thermal image super resolution. In: *CVPR*. pp. 94–95 (2020) [4](#)

37. Khaleghi, L., Sepas-Moghaddam, A., Marshall, J., Etemad, A.: Multi-view video-based 3D hand pose estimation. *IEEE Transactions on Artificial Intelligence* (2022) 4
38. Khattak, S., Papachristos, C., Alexis, K.: Keyframe-based thermal-inertial odometry. *Journal of Field Robotics* **37**(4), 552–579 (2020) 4
39. Kim, D.U., Kim, K.I., Baek, S.: End-to-end detection and pose estimation of two interacting hands. In: *ICCV*. pp. 11189–11198 (2021) 4
40. Kim, N., Choi, Y., Hwang, S., Kweon, I.S.: Multispectral transfer network: Unsupervised depth estimation for all-day vision. In: *AAAI* (2018) 4
41. Kim, Y.H., Shin, U., Park, J., Kweon, I.S.: MS-UDA: Multi-spectral unsupervised domain adaptation for thermal image semantic segmentation. *RA-L* **6**(4), 6497–6504 (2021) 4
42. Kirillov, A., Mintun, E., Ravi, N., Mao, H., Rolland, C., Gustafson, L., Xiao, T., Whitehead, S., Berg, A.C., Lo, W.Y., et al.: Segment anything. *arXiv preprint arXiv:2304.02643* (2023) 8
43. Kocabas, M., Athanasiou, N., Black, M.J.: VIBE: Video Inference for Human Body Pose and Shape Estimation. In: *CVPR* (June 2020) 4
44. Kütük, Z., Algan, G.: Semantic segmentation for thermal images: A comparative survey. In: *CVPR*. pp. 286–295 (2022) 4
45. Kwon, T., Tekin, B., Stühmer, J., Bogó, F., Pollefeys, M.: H2o: Two hands manipulating objects for first person interaction recognition. In: *ICCV*. pp. 10138–10148 (2021) 3, 4, 7, 10, 14
46. Li, C., Xia, W., Yan, Y., Luo, B., Tang, J.: Segmenting objects in day and night: Edge-conditioned CNN for thermal image semantic segmentation. *TNNLS* **32**(7), 3069–3082 (2020) 4
47. Li, M., An, L., Zhang, H., Wu, L., Chen, F., Yu, T., Liu, Y.: Interacting attention graph for single image two-hand reconstruction. In: *CVPR*. pp. 2761–2770 (2022) 1, 4
48. Liang, H., Yuan, J., Thalmann, D., Thalmann, N.M.: Ar in hand: Egocentric palm pose tracking and gesture recognition for augmented reality applications. In: *ACM MM*. pp. 743–744 (2015) 1, 3
49. Lin, F., Wilhelm, C., Martinez, T.: Two-hand global 3d pose estimation using monocular rgb. In: *WACV*. pp. 2373–2381 (2021) 1, 4
50. Liu, R., Vondrick, C.: Humans as Light Bulbs: 3D Human Reconstruction from Thermal Reflection. In: *CVPR*. pp. 12531–12542 (2023) 4
51. Liu, S., Jiang, H., Xu, J., Liu, S., Wang, X.: Semi-supervised 3d hand-object poses estimation with interactions in time. In: *CVPR*. pp. 14687–14697 (2021) 4
52. Liu, Y., Liu, Y., Jiang, C., Lyu, K., Wan, W., Shen, H., Liang, B., Fu, Z., Wang, H., Yi, L.: HOI4D: A 4D egocentric dataset for category-level human-object interaction. In: *CVPR*. pp. 21013–21022 (2022) 3, 4, 14
53. LLC, G.: MediaPipe Hands. <https://github.com/google/mediapipe> (2020), accessed: 2024-02-13 7
54. Lloyd, J.M.: *Thermal imaging systems*. Springer Science & Business Media (2013) 2, 4
55. Lu, Y., Lu, G.: An alternative of lidar in nighttime: Unsupervised depth estimation based on single thermal image. In: *WACV*. pp. 3833–3843 (2021) 4
56. Lupión, M., Polo-Rodríguez, A., Medina-Quero, J., Sanjuan, J.F., Ortigosa, P.M.: 3D Human Pose Estimation from multi-view thermal vision sensors. *Information Fusion* **104**, 102154 (2024) 4
57. Marchand, E., Uchiyama, H., Spindler, F.: Pose estimation for augmented reality: a hands-on survey. *TVCG* **22**(12), 2633–2651 (2015) 1, 3

58. Meta: Meta Quest. <https://www.meta.com/gb/quest/> (2024), accessed: 2024-02-23 **1**
59. Moon, G., Chang, J.Y., Lee, K.M.: V2v-posenet: Voxel-to-voxel prediction network for accurate 3d hand and human pose estimation from a single depth map. In: CVPR. pp. 5079–5088 (2018) **4**
60. Moon, G., Yu, S.I., Wen, H., Shiratori, T., Lee, K.M.: Interhand2. 6m: A dataset and baseline for 3d interacting hand pose estimation from a single rgb image. In: ECCV. pp. 548–564. Springer (2020) **3, 4, 11, 14**
61. Mueller, F., Bernard, F., Sotnychenko, O., Mehta, D., Sridhar, S., Casas, D., Theobalt, C.: Gnerated hands for real-time 3d hand tracking from monocular rgb. In: CVPR. pp. 49–59 (2018) **3**
62. Mueller, F., Davis, M., Bernard, F., Sotnychenko, O., Verschoor, M., Otaduy, M.A., Casas, D., Theobalt, C.: Real-time pose and shape reconstruction of two interacting hands with a single depth camera. TOG **38**(4), 1–13 (2019) **3**
63. Mueller, F., Mehta, D., Sotnychenko, O., Sridhar, S., Casas, D., Theobalt, C.: Real-time hand tracking under occlusion from an egocentric rgb-d sensor. In: ICCV. pp. 1154–1163 (2017) **3, 4**
64. Ohkawa, T., He, K., Sener, F., Hodan, T., Tran, L., Keskin, C.: AssemblyHands: Towards Egocentric Activity Understanding via 3D Hand Pose Estimation. In: CVPR. pp. 12999–13008 (2023) **3, 4, 14**
65. Park, J., Oh, Y., Moon, G., Choi, H., Lee, K.M.: Handocnet: Occlusion-robust 3d hand mesh estimation network. In: CVPR. pp. 1496–1505 (2022) **4**
66. Qin, Y., Wu, Y.H., Liu, S., Jiang, H., Yang, R., Fu, Y., Wang, X.: Dexmv: Imitation learning for dexterous manipulation from human videos. In: ECCV. pp. 570–587. Springer (2022) **1, 4**
67. Rivadeneira, R.E., Sappa, A.D., Vintimilla, B.X., Bin, D., Ruodi, L., Shengye, L., Zhong, Z., Liu, X., Jiang, J., Wang, C.: Thermal Image Super-Resolution Challenge Results-PBVS 2023. In: CVPR. pp. 470–478 (2023) **4**
68. Romero, J., Tzionas, D., Black, M.J.: Embodied Hands: Modeling and Capturing Hands and Bodies Together. TOG **36**(6) (2017) **2, 3, 4, 7, 11**
69. Sagayam, K.M., Hemanth, D.J.: Hand posture and gesture recognition techniques for virtual reality applications: a survey. Virtual Reality **21**, 91–107 (2017) **1, 3**
70. Sage, A., Ledwoń, D., Juszczak, J., Badura, P.: 3D Thermal Volume Reconstruction from 2D Infrared Images—a Preliminary Study. In: Innovations in Biomedical Engineering. pp. 371–379. Springer (2021) **4**
71. Sampieri, A., di Melendugno, G.M.D., Avogaro, A., Cunico, F., Setti, F., Skenderi, G., Cristani, M., Galasso, F.: Pose forecasting in industrial human-robot collaboration. In: ECCV. pp. 51–69. Springer (2022) **1, 3**
72. Saputra, M.R.U., de Gusmao, P.P., Lu, C.X., Almalioglu, Y., Rosa, S., Chen, C., Wahlström, J., Wang, W., Markham, A., Trigoni, N.: Deeptio: A deep thermal-inertial odometry with visual hallucination. RA-L **5**(2), 1672–1679 (2020) **4**
73. Saputra, Muhamad Risqi U. and Lu, Chris Xiaoxuan and de Gusmao, Pedro Porto B. and Wang, Bing and Markham, Andrew and Trigoni, Niki: Graph-based thermal-inertial slam with probabilistic neural networks. TRO **38**(3), 1875–1893 (2022) **4**
74. Schramm, S., Osterhold, P., Schmoll, R., Kroll, A.: Combining modern 3D reconstruction and thermal imaging: Generation of large-scale 3D thermograms in real-time. Quantitative InfraRed Thermography Journal **19**(5), 295–311 (2022) **4**
75. Seewald, L.A., Rodrigues, V.F., Ollenschläger, M., Antunes, R.S., da Costa, C.A., da Rosa Righi, R., da Silveira Jr, L.G., Maier, A., Eskofier, B., Fahrig, R.: To-

- ward analyzing mutual interference on infrared-enabled depth cameras. *Computer Vision and Image Understanding* **178**, 1–15 (2019) [1](#)
76. Sener, F., Chatterjee, D., Shelepov, D., He, K., Singhania, D., Wang, R., Yao, A.: Assembly101: A large-scale multi-view video dataset for understanding procedural activities. In: *CVPR*. pp. 21096–21106 (2022) [3](#)
 77. Shin, U., Lee, K., Lee, S., Kweon, I.S.: Self-supervised depth and ego-motion estimation for monocular thermal video using multi-spectral consistency loss. *RA-L* **7**(2), 1103–1110 (2021) [4](#)
 78. Shin, U., Park, J., Kweon, I.S.: Deep Depth Estimation From Thermal Image. In: *CVPR*. pp. 1043–1053 (June 2023) [4](#)
 79. Shin, Y.S., Kim, A.: Sparse depth enhanced direct thermal-infrared SLAM beyond the visible spectrum. *RA-L* **4**(3), 2918–2925 (2019) [4](#)
 80. Smith, B., Wu, C., Wen, H., Peluse, P., Sheikh, Y., Hodgins, J.K., Shiratori, T.: Constraining dense hand surface tracking with elasticity. *TOG* **39**(6), 1–14 (2020) [4](#)
 81. Smith, J., Loncomilla, P., Ruiz-Del-Solar, J.: Human Pose Estimation using Thermal Images. *IEEE Access* (2023) [4](#)
 82. Spurr, A., Iqbal, U., Molchanov, P., Hilliges, O., Kautz, J.: Weakly supervised 3d hand pose estimation via biomechanical constraints. In: *ECCV*. pp. 211–228. Springer (2020) [4](#)
 83. Sridhar, S., Mueller, F., Zollhöfer, M., Casas, D., Oulasvirta, A., Theobalt, C.: Real-time joint tracking of a hand manipulating an object from rgb-d input. In: *ECCV*. pp. 294–310. Springer (2016) [3](#)
 84. Suarez, J., Murphy, R.R.: Using the kinect for search and rescue robotics. In: *SSRR*. pp. 1–2. IEEE (2012) [1](#)
 85. Taheri, O., Ghorbani, N., Black, M.J., Tzionas, D.: GRAB: A dataset of whole-body human grasping of objects. In: *ECCV*. pp. 581–600. Springer (2020) [3](#)
 86. Tech, T.: Testing the Apple Vision Pro in Pitch Black Environments. YouTube (2024), https://www.youtube.com/watch?v=w1Ppo_QFIRU [1](#)
 87. Teledyne FLIR: Boson - Uncooled, Longwave Infrared (LWIR) OEM Thermal Camera Module (2024), <https://www.flir.co.uk/products/boson/?model=20640AS95-6IARX&vertical=lwir&segment=oem>, accessed: 2024-02-13 [5](#)
 88. Vaswani, A., Shazeer, N., Parmar, N., Uszkoreit, J., Jones, L., Gomez, A.N., Kaiser, Ł., Polosukhin, I.: Attention is all you need. *NIPS* **30** (2017) [10](#)
 89. Vertens, J., Zürn, J., Burgard, W.: Heatnet: Bridging the day-night domain gap in semantic segmentation with thermal images. In: *IROS*. pp. 8461–8468. IEEE (2020) [4](#)
 90. Vizzo, I., Guadagnino, T., Mersch, B., Wiesmann, L., Behley, J., Stachniss, C.: Kiss-icp: In defense of point-to-point icp—simple, accurate, and robust registration if done the right way. *RA-L* **8**(2), 1029–1036 (2023) [6](#)
 91. Wang, J., Mueller, F., Bernard, F., Sorli, S., Sotnychenko, O., Qian, N., Otaduy, M.A., Casas, D., Theobalt, C.: Rgb2hands: real-time tracking of 3d hand interactions from monocular rgb video. *TOG* **39**(6), 1–16 (2020) [4](#)
 92. Wen, Y., Pan, H., Yang, L., Pan, J., Komura, T., Wang, W.: Hierarchical temporal transformer for 3d hand pose estimation and action recognition from egocentric rgb videos. In: *CVPR*. pp. 21243–21253 (2023) [1](#), [4](#), [11](#), [12](#), [13](#)
 93. Wu, M.Y., Ting, P.W., Tang, Y.H., Chou, E.T., Fu, L.C.: Hand pose estimation in object-interaction based on deep learning for virtual reality applications. *J. Vis. Commun. Image Represent.* **70**, 102802 (2020) [1](#), [3](#)

94. Xiong, F., Zhang, B., Xiao, Y., Cao, Z., Yu, T., Zhou, J.T., Yuan, J.: A2j: Anchor-to-joint regression network for 3d articulated pose estimation from a single depth image. In: Proceedings of the IEEE/CVF International Conference on Computer Vision. pp. 793–802 (2019) [4](#)
95. Yang, J., Chang, H.J., Lee, S., Kwak, N.: SeqHAND: RGB-sequence-based 3D hand pose and shape estimation. In: ECCV. pp. 122–139. Springer (2020) [4](#)
96. Yang, L., Yao, A.: Disentangling latent hands for image synthesis and pose estimation. In: CVPR. pp. 9877–9886 (2019) [4](#)
97. Yuan, S., Ye, Q., Stenger, B., Jain, S., Kim, T.K.: Bighand2. 2m benchmark: Hand pose dataset and state of the art analysis. In: CVPR. pp. 4866–4874 (2017) [3](#), [4](#)
98. Zhang, B., Wang, Y., Deng, X., Zhang, Y., Tan, P., Ma, C., Wang, H.: Interacting two-hand 3d pose and shape reconstruction from single color image. In: ICCV. pp. 11354–11363 (2021) [4](#)
99. Zhang, X., Li, Q., Mo, H., Zhang, W., Zheng, W.: End-to-end hand mesh recovery from a monocular rgb image. In: ICCV. pp. 2354–2364 (2019) [4](#)
100. Zhang, Z., Xie, S., Chen, M., Zhu, H.: HandAugment: A simple data augmentation method for depth-based 3D hand pose estimation. arXiv preprint arXiv:2001.00702 (2020) [4](#)
101. Zhu, T., Sun, Y., Ma, X., Lin, X.: Hand Pose Ensemble Learning Based on Grouping Features of Hand Point Sets. In: ICCVW (2019) [4](#)
102. Zhu, X., Su, W., Lu, L., Li, B., Wang, X., Dai, J.: Deformable detr: Deformable transformers for end-to-end object detection. In: ICLR (2020) [9](#)
103. Zimmermann, C., Brox, T.: Learning to estimate 3d hand pose from single rgb images. In: ICCV. pp. 4903–4911 (2017) [3](#), [11](#)
104. Zimmermann, C., Ceylan, D., Yang, J., Russell, B., Argus, M., Brox, T.: Freihand: A dataset for markerless capture of hand pose and shape from single rgb images. In: ICCV. pp. 813–822 (2019) [3](#), [4](#), [10](#)